Energy 36 (2011) 1749–1757

Contents lists available at ScienceDirect

Energy

journal homepage: www.elsevier.com/locate/energy

New silicon thin-film technology associated with original DC–DC converter: An economic alternative way to improve photovoltaic systems efficiencies

F. Dadouche [b,*], O. Béthoux [a], J-P. Kleider [a]

[a] Laboratoire de Génie Electrique de Paris, CNRS UMR8507, SUPELEC, Université Paris-Sud, UPMC-Université Paris 6, 11 rue Joliot Curie, Plateau de Moulon, F-91192 Gif-sur-Yvette Cedex, France
[b] Institut d'Électronique du Solide et des Systèmes (InESS), 23 rue Loess BP 20 CR, F-67037 STRASBOURG Cedex 2, France

ARTICLE INFO

Article history:
Received 17 June 2010
Received in revised form
20 November 2010
Accepted 22 December 2010
Available online 4 January 2011

Keywords:
Silicon thin film solar cells
Tandem 4-wires structure
DC–DC-converter

ABSTRACT

In this article, we aim at optimizing an innovative tandem structure based on polymorphous and microcrystalline silicon for the top and bottom elementary cells, respectively, combined with an original DC–DC converter.

The studied tandem structure is composed of two cells, each being connected to its own separate electrodes making the structure electrically decoupled but optically coupled. In those conditions, the constraint of current matching usually needed in the classical micromorph structures is avoided. As a result, the robustness against the current variations is enhanced and the efficiency of the structure is improved.

Since the top cell plays the main role in the determination of the transmitted part of the incoming flux to the bottom cell, the thickness of the intrinsic layer of the polymorphous cell is tuned so that the output power of the global structure becomes maximal.

To implement the electric decoupling of two sub cells, the studied structure needs two static converters. In order to minimize the converters bulk, we design an innovative output electric architecture and its optimized related control signals.

1. Introduction

Energy is central to achieving the interrelated economic, social, and environmental aims of sustainable human development. Due to limited fossil fuel supplies as well as increased concerns over environmental preservation, the need for alternative methods of power generation has become increasingly important [1]. Recently, global warming has become one of the world wide problems. Therefore some measure for reduction of carbon dioxide emissions is the most urgent and important subject because it is produced in large quantity by fossil fuels combustion and is considered as the principal origin of the greenhouse effect. The CO_2 emission has to be reduced by a factor of 50–80% by the year 2050 [2,3].

Renewable energies (RE), in particular solar energy, are needed to meet the growing electricity demand and at the same time to take care of the shrinking fossil resources and to reduce global CO_2 emissions. As a matter of fact, the sun represents an inexhaustible and abundant energy source, providing the earth with a huge power of 1.6×10^9 TWh/year [4]. The amount of the world final energy consumption has nearly doubled within three decades: 54195 TWh in 1973 compared to 93774 TWh in 2006 [5]. The electricity share within the same period has jumped from 9.4% to 16.7%. Over a population of 6 Billion, 1.8 Billion do not have access to electricity (30% of the world population, 50% Arab world); 25% of the world population consume more than 75% of the total world energy supply. Admittedly, the future might not see the same degree of dependence on oil and gas as alternative and renewable energy sources should be employed to close the supply-demand gap.

Solar photovoltaics (PV) systems are among the most promising electrical generation technologies to emerge in recent decades. They are qualified as being economically viable, environmentally friendly, sustainable, and socially equitable solution to modern society's energy requirements [6,7].

Just over 50 years ago, this solar-electricity technology marked a significant modern tipping point at Bell Telephone Laboratories when Daryl Chapin, Gerald Pearson, and Calvin Fuller suddenly turned a research curiosity into a viable electricity producer. Their research innovation brought the performances of these crystalline silicon devices from "laboratory interest" (conversion efficiencies hovering at 1%) to efficiencies 5–8 times greater, earning their

* Corresponding author. Tel.: +33 (0)3 88 10 62 59; fax: +33 (0)3 88 10 65 48.
E-mail address: foudil.dadouche@iness.c-strasbourg.fr (F. Dadouche).

0360-5442/$ – see front matter © 2011 Elsevier Ltd. All rights reserved.
doi:10.1016/j.energy.2010.12.054

Nomenclature

a-Si:H	Hydrogenated amorphous silicon
Cd	Cadmium
CdTe	Cadmium telluride
CIGS	Copper Indium Gallium (di) Selenide
Ge	Germanium
In	Indium
I-layer	"Intrinsic" layer (nominally undoped)
J–V	Current density–Voltage characteristic
MPPT	Maximum Power Point Tracking
N-layer	*n*-type doped layer
PECVD	Plasma Enhanced Chemical Vapor Deposition
P-layer	*p*-type doped layer
pm-Si:H	Hydrogenated polymorphous silicon
P–V	Power density–Voltage characteristic
PWM	Pulse Width Modulated
RF	Radio Frequency
Se	Selenium
Si	Silicon
Te	Tellurium
μc-Si:H	Hydrogenated microcrystalline silicon

consideration as real electrical power sources. The PV industrial emergence began in the early 1960s because solar cells could provide reliable power for remote applications such as space vehicles, off-grid villages, remote telephone relays, emergency call boxes, etc. Photovoltaic worldwide production is recently dedicated to grid applications [8], which leads to a major evolution of PV industry and a great increase of the installed capacity. For instance, the European installed capacity has increased from 4279 MWp in 2007 to 7910 MWp in 2008 and PVs are estimated to provide about 12% of the European electricity consumption by 2020 [9,10].

PV value is straightforward and truly the power of choice for grid connection that provide a more stable energy environment and economy if new challenged are taken into account in that: it has to reduce drastically the cost of produced peak power and reaching high production level which implies the development of industrial processes exclusively based on abundant materials such as Silicon (Si) [11].

PV technology includes a number of significant component performance "gaps" for various crystalline, polycrystalline, and amorphous; bulk, as well as thin-film technologies. Monocrystalline Si cell technology is becoming mature with high electrical efficiency of 13–15%. As far as raw materials and cost effectiveness are concerned, monocrystalline Si PV technologies appear to be limited in mass production because of a quite high process cost [12] and the use of silver in the electric contact electrode. Moreover, thin film technologies growth (CIGS and CdTe) will be limited mainly by the availability and/or the toxicity of different materials composing this technology (e.g., Te, In, Ge, Cd and Se) [12,13]. Finally, thin-film silicon solar cells technologies could reach the terawatt production level as claimed in the IPCC report [14].

This expected result is supported by the numerous researches which have allowed to reach high deposition rates combined with good quality silicon thin films using different deposition techniques [15–18] leading to higher efficiency solar cells. In addition this technology seems to be more interesting in term of cost and CO_2 emission than the classical monocrystalline one [9,19]. However, when using PECVD method, the prevalent form of silicon obtained is hydrogenated amorphous silicon (a-Si:H), which presents two drawbacks. Firstly, the energy bandgap is slightly too high (1.7–1.8 eV) [20] to convert a high portion of near infrared photons that are present in the solar spectrum [21]. Secondly, the amorphous network leads to chemical bonding defects in the material structure: weak Si–Si bonds and dangling bonds. In addition, it is now well known that additional defects are created under light effect [22], leading to a degradation of solar cell efficiency during the first months of operation.

Many researches have been devoted to improve amorphous silicon electronic properties. This has led to new promising silicon materials: hydrogenated polymorphous silicon (pm-Si:H) and hydrogenated microcrystalline silicon (μc-Si:H). These two semiconductors generally are produced by low temperature PECVD techniques like for a-Si:H, thus sharing the same facilities and large area production potential. In order to be capable of processing such materials, deposition conditions have to be monitored. Microcrystalline silicon is generally fabricated at low pressure and needs higher hydrogen content in the gas mixture. It has a lower bandgap than a-Si:H, and exhibits almost no light induced degradation. Polymorphous silicon is a heterogeneous material processed at higher pressure and higher power in a regime close to the powder regime, where nanoparticles formed in the plasma are deposited onto the substrate and embedded in an amorphous matrix [23–27]. It has been shown that pm-Si:H has a lower defect density than a-Si:H, and a better stability, while the bandgap energy is slightly larger [15].

Besides their promising electronic qualities, the use of both pm-Si:H and μc-Si:H allows us to cover a larger spectral range compared to that of a-Si:H and therefore increase the electric output of the PV modules. This has led to the proposition of combining, in a tandem structure, of two elementary cells made respectively of μc-Si:H (called bottom cell) and pm-Si:H (called top cell). This kind of thin film Si multijunction solar cells is considered, in our work, to be a potential method leading to new way of integrating the power electronics devices close to the modules.

The aim of this article is to present a system that combines a tandem structure solar cell with an original static converter as well as a simulation procedure adopted to optimize the studied structure.

2. Studied structure

The tandem cell concept consists in putting together in the same structure two solar cells made of materials that have different bandgap energies, for a better matching of the bandgap and incoming photons energy. The bottom cell is made of materials with a low bandgap such as microcrystalline silicon and the top cell materials have higher bandgap such as amorphous and polymorphous silicon. This structure permits to extend the spectral range of high collection efficiency [27]. Indeed the top cell has a better photo response in the blue region while the bottom cell is more efficient in the red and infrared regions.

In previous work, we have already discussed the best choice for cells connection in tandem structures [26]. Two ways of associating the cells were studied and compared: (i) the classical structure in which the two cells are electrically and optically coupled, called the 2-wires structure, and (ii) an innovative structure for which the electrical constraint is relaxed by the electrical decoupling of the two cells, called the 4-wires structure. Our study led to the conclusion that the 4-wires structure is, in any case, better than the traditional 2-wires one. Moreover, we can argue a much more robust maximum power point. So the structure selected to be studied in this work is the 4-wires one. It consists of two independent cells, each of theme needs its own two electrodes connected to its P and N layers (Fig. 1a). The advantage of this structure compared to the classical one, made by a successive layer deposition (Fig. 1b), is that the two sub cells can work with different currents and so there is no need to match their currents. This leads to a more efficient structure.

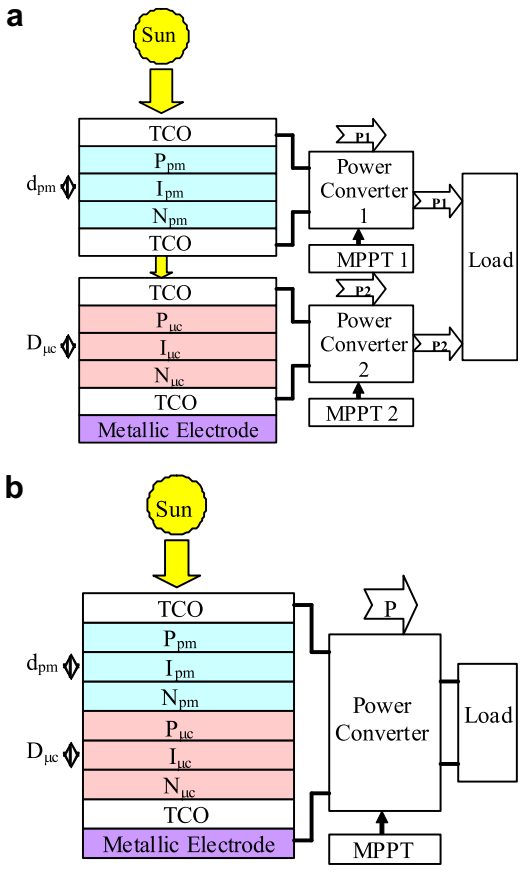

Fig. 1. Two kinds of tandem connection and the associated power converter: (a) 4-wires structure (b) 2-wires structure.

In this work the top cell is made of pm-Si:H because of its proven better electronic properties and better stability compared to the conventional a-Si:H [28–31]. In addition the optical bandgap of pm-Si:H is slightly larger than the a-Si:H one.

The pm-Si:H is characterized by a high absorption index thus it requires a few hundreds thin active layer to convert its useful spectrum [300 nm–720 nm]. In contrast, the μm-Si:H cell has a lower absorption coefficient which imposes a wider intrinsic layer.

3. Associated static converter

As the two cells of this considered structure (4-wires) are electrically decoupled, this design needs a dedicated architecture to add the electric powers provided by the top and the bottom cells. Thus, each sub-cell supplies its power to the external load through an associated power converter. This enables both blocks, made of sub-cell and sub-converter, having either the same current (which leads to series connection) and the same voltage (which leads to parallel connection).

The converter can be either a voltage step-up (boost converter) or a voltage step-down (buck converter) device. As PV cells are low voltage power sources and loads are high voltage devices, and in order to reduce Joule effect losses, it is mandatory to use a boost converter at the output of a PV module. The two independent boost converters can be associated either in parallel or in series (Fig. 2). Each connection is suitable for independent power tracking.

In the parallel case, each MPPT algorithm computes the controlled switch PWM duty cycle d_k that enables its cell to work at its maximum power point:

$$d_k = 1 - \frac{(V_{PVk})_{MPP}}{V_O} \quad (1)$$

Where V_O is the regulated load voltage.

As the maximum power voltage range is not so large, the duty cycle range is not considerable, which is a good point for power converter design optimization.

In the series case, each MPPT algorithm also computes its PWM duty cycle d_k independently, but, in this circumstance, d_k value is determined as follows:

$$d_k = 1 - \frac{(V_{PVk})_{MPP}}{(V_O)_k} \quad (2)$$

with $(V_O)_k$ the output voltage of each converter which can be calculated by a power balance:

$$(V_O)_k = \frac{(P_{PVk})_{MPP}}{P_O} V_O \quad (3)$$

Hence, in case of cells mismatching (ageing effects, environmental conditions as temperature or light spectrum…), $(V_O)_k$ can vary a lot inducing a duty cycle wide range which is negative as far as power device design is concerned (with respect to control and power efficiency). Consequently, this study is based on the parallel connection of boost converters.

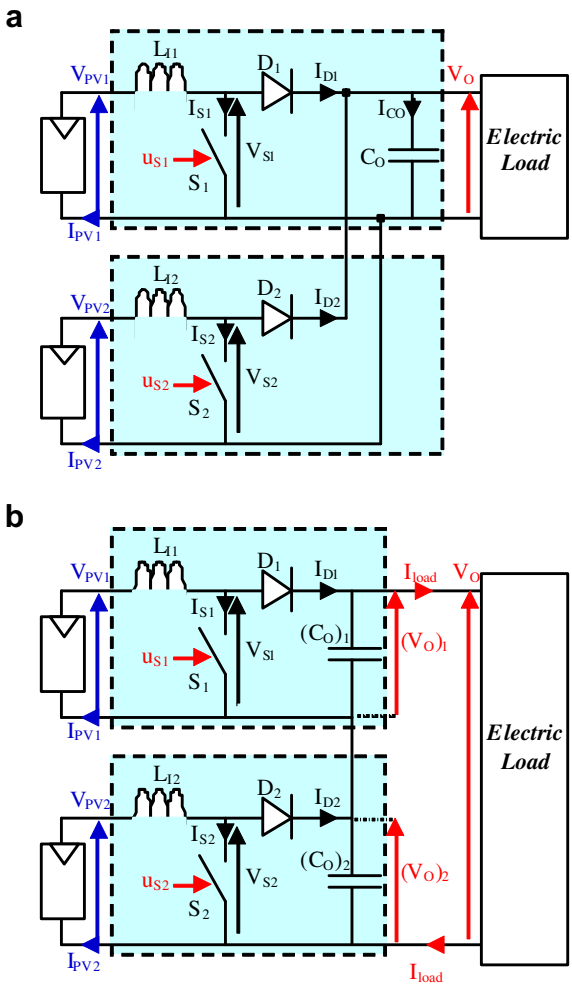

Fig. 2. Two types of power converter connections: (a) boost converters in parallel (b) boost converters in series.

4. Simulation tools and procedure

The simulation of the studied structure is performed in two successive steps using two different tools. First the pm-Si:H/μc-Si:H structure, without its associated converter, is optimized so that it produces the maximum power. Then, after computing the corresponding output current and voltage for both top and bottom cells, we design the associated optimized converter.

To optimize the studied structure and evaluate its output power we mainly used numerical simulation software developed by the Hahn-Meitner Institut (now Helmholtz Zentrum) in Berlin. The software called "AFORS-HET" (Automat FOR Simulation of HETerostructures) is dedicated to heterojunction solar cells [32]. It allows extracting different macroscopic characteristics in dark conditions or under sun illumination. For each structure, it enables to introduce different profiles of defects in the energy bandgap of each layer forming the cell.

In order to optimize the electrical architecture (boost converters connected in parallel), the widespread matlab/simulink interface is used. It allows implementing both any control law (MPPT in our case) and any converter (currently boost converter) by taking advantage of the power dedicated toolbox called "Sim Power Systems library". It also facilitates curves drawing and waveform analyses (Fast Fourier Transform, etc.) [33].

4.1. Optimization of pm-Si:H/μc-Si:H structure

The first step consists in tuning the thicknesses of the different layers of the top and bottom cells in order to obtain the maximum output power of the structure. The incident flux first goes through the top pm-Si:H cell, which absorbs part of the photons and transmits the remaining part to the bottom cell. Consequently, the top cell plays the main role and the thickness of its active I-layer must be determined accurately. The role of the P- and N- layers is to create the junctions and the internal electrical field through the intrinsic layers with a minimum of absorption, so they must be chosen as thin as possible. For the thickness of the microcrystalline intrinsic layer, it can be fixed to reasonable value, sufficiently large to absorb most of the output flux coming from the top cell. For silicon thin film tandem structures, this layer width is generally larger than one micron, so it is fixed at 1.5 μm. The thicknesses of all the layers are given in Table 1.

The key factor determining the thickness of the intrinsic layer of the pm-Si:H cell is the ageing process happening during the first months of illumination, called light-soaking. It is known that amorphous silicon thin films are characterized by two kinds of defects: the network defects linked to the weak bonds and the deep defects linked to the dangling bonds. According to the Staebler-Wronsky effect, under illumination, some weak bonds are broken leading to the creation of new dangling bonds [22].

The first kind of defects is usually modelled by two exponential bandtails situated in both sides of the bandgap. The second one, even if it is known to be of amphoteric type [34], can be modelled by two Gaussian continuous distributions of monovalent states [35,36].

In order to account for the light-soaking phenomenon on the performance of the pm-Si:H cell, we modelled the creation of new dangling bonds by increasing the magnitude of the Gaussian distributions (D_{max}) without varying their widths.

Fig. 3 illustrates the variations of pm-Si:H cell efficiency against the pm-Si:H intrinsic layer thickness for different values of D_{max} introduced in the simulation. It can be observed the decrease of the cell efficiency by increasing D_{max} for a given thickness. This is mainly due to the decrease of carrier diffusion length and screening of the electric field when the density of deep defects is increased. In addition and for a given D_{max} the cell efficiency first increases with the increase of the intrinsic layer thickness up to an optimal value, and then decreases (the decrease occurs at larger thickness for the lowest defect density and is not visible on this figure). This is due to two phenomena acting concurrently: (i) on the one hand the widening of the intrinsic layer leads to the increase of photogenerated carriers (ii) the probability for the created carriers to recombine before reaching the electrodes becomes higher. Therefore, the optimal thickness decreases since the defect density is increased.

From this simulation the location of the optimal thickness is determined for different states of the pm-Si:H materials as reported in Table 2.

Admittedly and in order to take into account the degradation caused by light soaking, it is necessary to limit the thickness of the intrinsic layer of the pm-Si:H cell to values lower than 500 nm. With regards to this fact and to estimate the output power of the studied tandem structure, we optimized the intrinsic layer thickness of the top cell to be within the interval [50 nm–450 nm].

The procedure adopted to perform our simulation is illustrated in Fig. 4 and summarized as follows:

- Application of standard AM1.5 illumination as an input flux of the top pm-Si:H cell.
- Variation of the intrinsic layer thickness of the top cell from 50 nm to 450 nm with a step of 50 nm.
- Calculation of the output flux of the pm-Si:H cell for each thickness.
- This last one is introduced as an input flux of the μc-Si:H cell.
- Computation of J–V and P–V curves for both cells.

Table 1
Thicknesses of the different layers of pm-Si:H and μc-Si:H cells introduced in the simulation.

	pm-Si:H cell		μc-Si:H cell	
	Material	Thickness (nm)	Material	Thickness (nm)
P-Layer	a-SiC:H	15	μc-Si:H	25
I-layer	Pm-Si:H	Variable	μc-Si:H	1500
N-layer	a-Si:H	20	a-Si:H	20

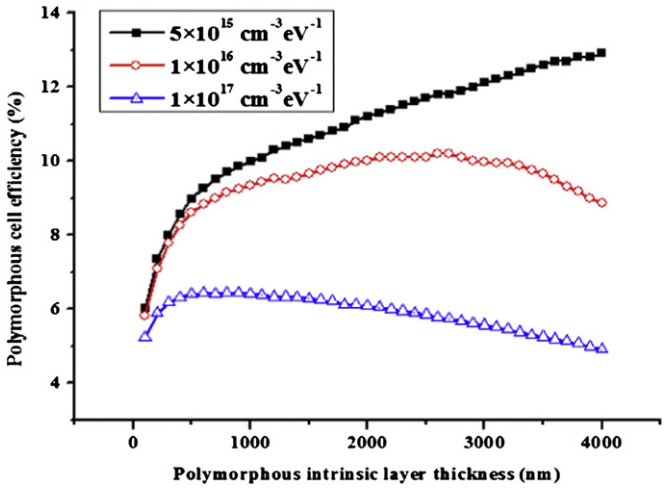

Fig. 3. pm-Si:H cell efficiency as a function of pm-Si:H intrinsic layer thickness for three values of the Gaussian distribution peak value D_{max}: 5×10^{15} cm^{-3} eV^{-1}, 1×10^{16} cm^{-3} eV^{-1}, 1×10^{17} cm^{-3} eV^{-1}.

Table 2
Optimal pm-Si:H thickness for the different material states.

State	D_{max} (cm^{-3} eV^{-1})	Optimal thickness (μm)
As deposited	5×10^{15}	Beyond 4
Intermediate	1×10^{16}	2.7
Light-soaked	1×10^{17}	0.3

Finally using the P–V curves, the maximum power is determined by adding the maximum power of elementary cells.

4.2. Static converter design and optimization

In order to improve the output efficiency of photovoltaic panels, it is important to operate the energy conversion systems near the maximum power point [37], so the objective of the control scheme is to track the maximum power point of both cells whatever the load requirements and the environmental conditions. For that purpose, the control algorithm can settle the PWM commands $u_{S1}(t)$ and $u_{S2}(t)$. These two variables provide three degrees of freedom. As a matter of fact, while operating at the same switching frequency F_S, they are characterized by their own duty cycles d_1 and d_2 as well as the phase shift $\phi_{1/2}$ between $u_{S1}(t)$ and $u_{S2}(t)$. As explained in section 3, the duty cycles d_1 and d_2 are computed in order to fulfil the maximum power requirements (eq. (1)).

The remaining degree of freedom $\phi_{1/2}$ can be used for further optimization. As the studied converters have to be integrated as close as possible to the photovoltaic module, their dimensions are a design key point. For this reason, it is important to minimize passive components size (inductors and capacitors). The boost output current $i_{Dk}(t)$ is a square shape with F_S frequency, (1-d_k) duty cycle and I_{PVk} magnitude. As any cyclic variable, $i_{Dk}(t)$ can be written as a Fourier series. The computation leads to the following expression:

$$i_{Dk}(t) = (1-d_k)I_k + 2(1-d_k)I_k \sum_{\ell=1}^{\infty} \frac{\sin(\ell d_k \pi)}{\ell d_k \pi} \cos(\ell \omega_S (t - T_k)) \tag{4}$$

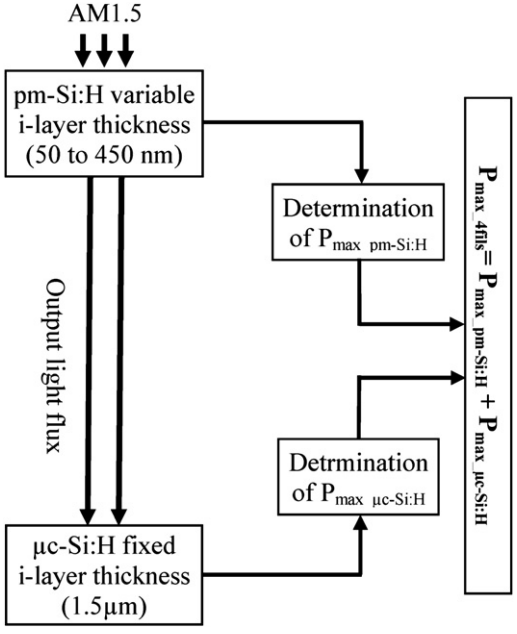

Fig. 4. Simulation steps for the 4-wires tandem structure.

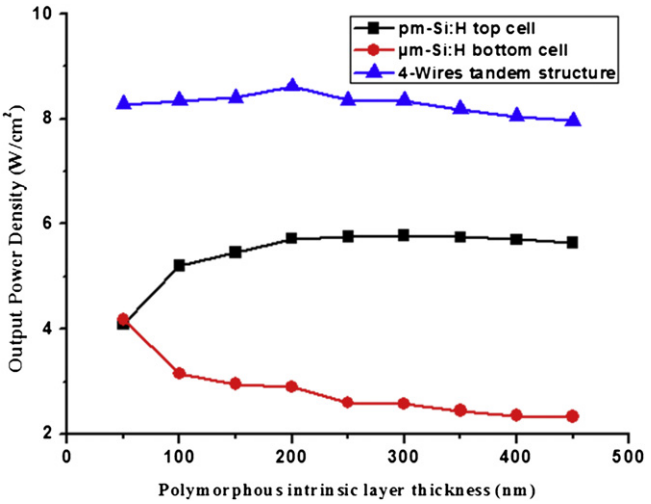

Fig. 5. Maximum outputs of elementary cells as well as the global tandem structure versus polymorphous intrinsic layer thickness.

Since the output capacitor function is to filter any switching frequencies, one can assume that its current is:

$$i_{CO}(t) = 2(1-d_1)I_1 \sum_{\ell=1}^{\infty} \frac{\sin(\ell d_1 \pi)}{\ell d_1 \pi} \cos(\ell \omega_S (t - T_1)) + 2(1-d_2)I_2 \times \sum_{\ell=1}^{\infty} \frac{\sin(\ell d_2 \pi)}{\ell d_2 \pi} \cos(\ell \omega_S (t - T_2)) \tag{5}$$

As capacitor filtering increases with frequency rise, the best choice is to minimize the first harmonic rank. This choice reduces any odd harmonic rank and settles the phase shift value ($\phi_{1/2}$) which is the last degree of freedom:

$$T_2 - T_1 = \frac{T_S}{2} \tag{6}$$

5. Results and discussion

The simulation results are divided in three sets: (i) the first concerns the studied structure including individual cells results after light soaking (ii) the second is dedicated to the associated

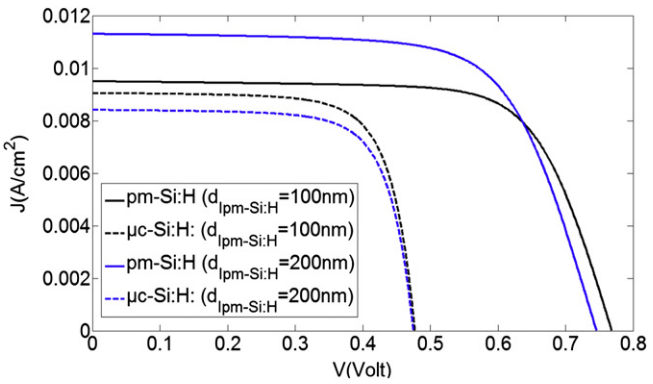

Fig. 6. J–V curves of both pm-Si:H and μc-Si:H cells and for different pm-Si:H I-layer thickness.

Table 3
Voltage and current values for the two elementary cells at the maximum power peak.

	$V_{MP\ peak}$ (mV)	$I_{MP\ peak}$ (mA)
pm-Si:H cell	567.5	10.08
µc-Si:H cell	386.2	7.52

converter (iii) the third part discusses the benefit of the converter panel integration.

5.1. Elementary cells and 4-wires structure results

For the first set, the maximum output power of the two sub cells as well as that of the global structure against the pm-Si:H intrinsic layer thickness are presented in Fig. 5. Then the electrical characteristics (J-V) curves of the top and bottom cells for two values of the top intrinsic layer thickness are reported on Fig. 6.

We can extract, from Fig. 5, the suitable thickness of the pm-S:H intrinsic layer to obtain the maximum output power of the structure. This depends on the performance of both top and bottom cells. For the top cell, as we have introduced it previously, and as a result

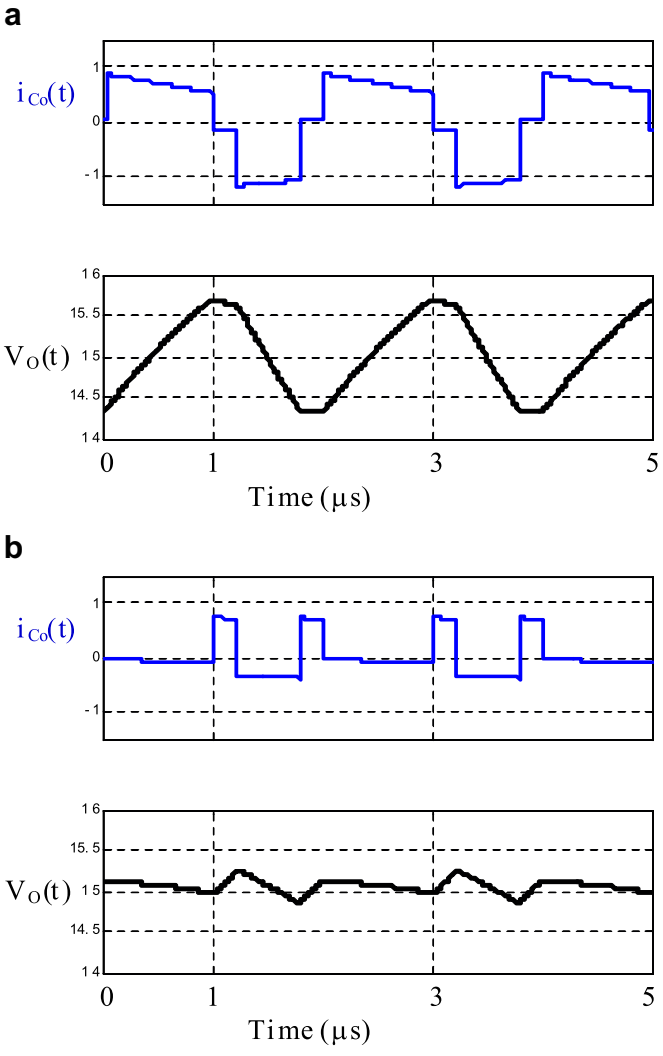

Fig. 7. Output capacitor current and voltage: (a) phase shift equal to 0 (b) phase shift equal to π.

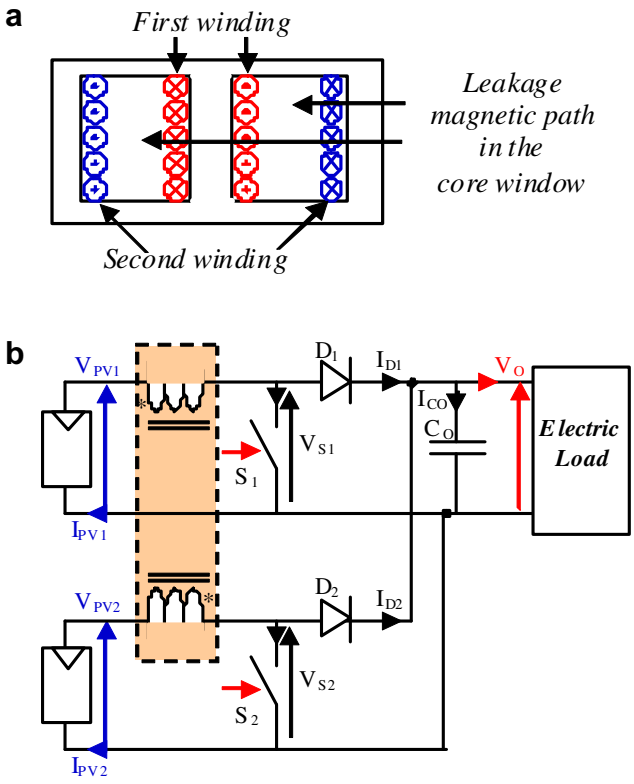

Fig. 8. The proposed power converter: (a) the coupled inductors (b) the interleaved power converter.

of the ageing process during light soaking, the light-soaked stabilized pm-Si:H cell presents an optimal value which is located in our case around 300 nm. However, since the microcrystalline cell is not affected by this process, its performance depends only on the fraction of flux transmitted by the top cell. Consequently, the thinner the top cell, the better the bottom cell efficiency. The combination of the two results explains that the optimal thickness for the pm-Si:H I-layer in the tandem structure is lower than for the pm-Si:H cell alone, and it is found to be around 200 nm.

A mismatching current in the two cells is observed when looking at the J–V curves of Fig. 6 at the already determined optimal thickness (200 nm). This means that to obtain the maximum power provided by the global structure it is necessary to exploit each cell independently. In addition and for a better electric power, the 4-wires structure is much more robust against current variations because it is no more constrained by the matching condition, as opposed to the classical 2-wires tandem structure, which is obviously more sensitive to current fluctuations caused by any outdoor conditions or manufacturing process.

5.2. Associated static converter results

In this section the simulation results of the electrical architecture are presented. This study is based on the previous values extracted from 4-wires structure simulations. As introduced before, the main parameters are the voltage and current of both cells corresponding to the maximum output power of the global structure. These values are summarized in the Table 3.

The following simulations are based on a top module made of twenty elementary top cells of roughly 1 A current output. The bottom module also consists of twenty elementary bottom cells of roughly 0.75 A. These values are calculated according to Table 3 and considering that both top and bottom cells have similar area.

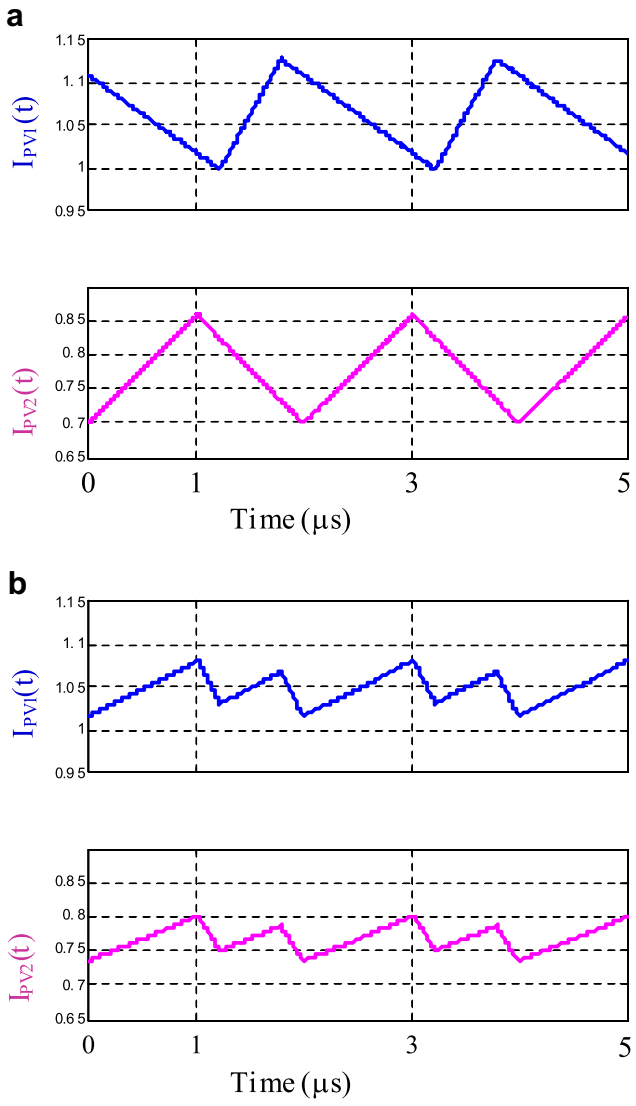

Fig. 9. Photovoltaic array currents: (a) with classic coil inductors (b) with intercell transformer.

The switching frequency F_S is fixed at 500 kHz, the inductors values are set to $L_{I1} = L_{I2} = 50$ µH and the output capacitor value is $C_O = 500$ nF. The variations of output capacitor current and voltage are reported on Fig. 7.

Figure 7-a illustrates an inappropriate tuning corresponding to a phase shift value of 0 and leading to a large current magnitude at the switching frequency F_S. However, Figure 7-b shows the optimal case; the phase shift value is equal to π. This set of control parameters leads to a much smaller current magnitude with a very small fundamental frequency F_S; the main harmonic component is obviously 2 F_S, a frequency which is hence twice easier to filter. That is the reason why the output voltage ripple is drastically reduced in this optimal case.

By choosing both parallel connection and interleaving technique of the control signals, it is possible to minimize the output filter (output capacitor) dimensions and improve efficiency. But the input part of the converter behaves as if there was a single converter. Therefore the interleaving technique does not lead to any current ripple decrease. In order to reduce the inductors bulk, these input inductors can be interlaced [38–42]. By building them on a same magnetic core, we introduce a transformer instead of two inductors (Fig. 8). This transformer is characterized by self inductances L_1 and L_2 and the mutual inductance M.

In this case, DC component and low frequency current are filtered by the leakage inductance. This last one is designed by choosing the leakage magnetic path in the winding core window. Most of the high frequency current (linked to switching ripples) are filtered by the mutual inductance which value is much larger than the basic inductor value. As a result this latter must have a low permeability material in order to store the DC energy ($1/2 \times LI^2$). Consequently, this chosen design leads to a small inductor value whereas the transformer doesn't face the same constraint.

The input current waveforms are reported on Fig. 9a; the signals present high current ripples at the switching frequency F_S. By integrating the two inductors into a same transformer, this frequency almost disappears and the current ripples magnitude is hence much smaller (Fig. 9b). The transformer has the same leakage inductance $L_{leakage} = 50$ µH, but its mutual inductance is much higher $M = 5$ mH.

5.3. Converter panel integration

In the previous section, we demonstrated that using a power converter based on coupled inductors leads to a smaller size device than the classical boost architecture. But from a system point of view, it is mandatory to ensure that the operating point of each panel remains as close as possible to its optimal value. That is the reason why we compare the output power of the two possible associations.

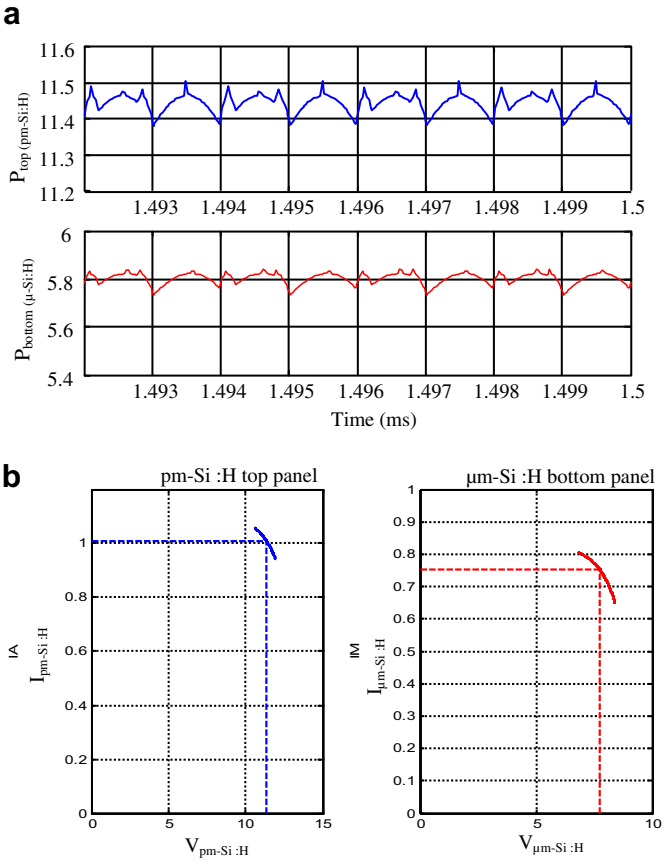

Fig. 10. Electrical output characteristics of top and bottom photovoltaic panels associated with their parallel boost converters controlled by interleaved PWM signals: (a) output power (b) operating point.

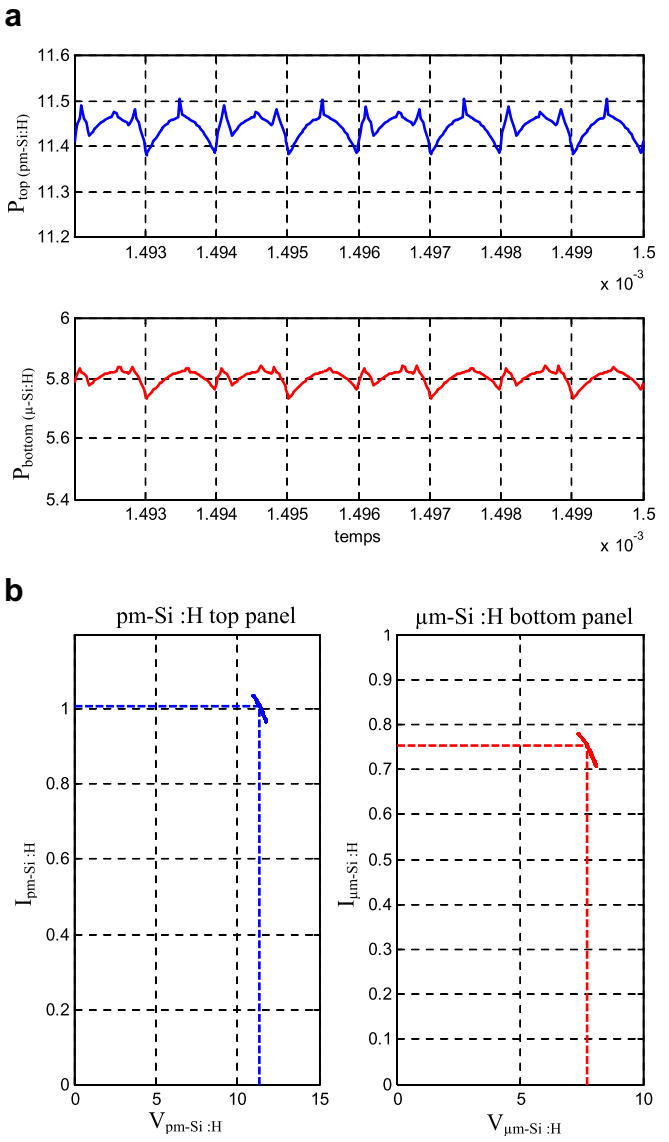

Fig. 11. Electrical output characteristics of top and bottom photovoltaic panels associated with coupled inductors boost converter controlled by interleaved PWM signals: (a) output power (b) operating point.

Fig. 10a shows the output power of pm-Si:H and µc-Si:H photovoltaic panels (top and bottom) connected to their own boost converters in a parallel mode association. Their PWM control signals are interleaved. It reveals significant power ripples around optimum for both panels. As a matter of fact, power converters have to work in switching mode inducing operating point fluctuations.

Fig. 10b illustrates that the operating point swings around the maximum power point (MPP) leading to a global power losses. One way to reduce this swing is to increase the PWM frequency. For instance, doubling the switching frequency would lead to divide the ripple magnitude by two. However, this solution induces converter loss increase.

The innovative method proposed in previous section, consisting in interconnecting both boost converters with the coupled inductor transformer as explained in Fig. 8, allows reducing the ripple without increasing switching frequency.

As it can be observed from Fig. 11a, the ripple magnitude is 2.3 times smaller than in the classical previous case. In addition the operating point remains closer to the MPP. As a result, without any further losses, the global system is more stable and has a smaller size.

6. Conclusion

It is clear that PV is the fastest growing electricity source over the past year and past five years, we have to provide the technical expertise, the resources, the creativity and innovation to keep the progress on. In this work a simulation study of an innovative tandem pm-Si:H/µc-Si:H structure associated to an original converter is performed.

Firstly, the structure is optimized in order to extract the maximum output power of each individual cell. Taking account of the light-soaking process, the optimal thickness of the intrinsic pm-Si:H layer in the top cell was found to be around 200 nm. For this thickness, we noticed a current mismatching between the two sub-cells. In order to achieve the best performance with different cell currents, it is mandatory to associate, for each cell, its own converter. In addition this implementation allows the global structure to be far less sensitive to operating conditions (temperature, light spectrum, etc). Thus the 4-wires structure is not constrained by the current matching condition which is mandatory in the case of a classical 2-wires tandem structure. This confirms the best performance of this structure and its robustness against current variations resulted from outdoor conditions or manufacturing process.

Secondly, this innovative tandem cell design is built in association with dedicated power converters. For this purpose, the different converters and their combinations are explored in order to design very compact electric output architecture. This leads to the choice of boost converters. In order to take advantage of the interleaving technique the converters outputs are associated in parallel. The innovative part of the study is that we have also associated the input inductors. This approach allows the converters to reduce their input filter bulk. Optimizing the boost control values by interleaving them, we therefore succeed to dramatically reduce both output capacitor value and input core size. The other advantage of the proposed architecture is that the operating point remains closer to the maximum power point (MPP) of the system.

Acknowledgements

This work was partly supported by ANR (Agence Nationale de la Recherche) in the framework of the ATOS project.

The authors are grateful to Professor Amine Boudghene Stambouli for fruitful discussions and critical reading of the manuscript as well as the constructive comments and suggestions.

References

[1] Lior N. Sustainable energy development: the present (2009) situation and possible paths to the future. Energy 2010;(35):3976–94.
[2] Hadjipaschalis I, Kourtis G, Poullikkas A. Assessment of oxyfuel power generation technologies. Renewable and Sustainable Energy Reviews 2009; 13:2637–44.
[3] Akorede MF, Hizam H, Pouresmaeil E. Distributed energy resources and benefits to the environment. Renewable and Sustainable Energy Reviews 2010;14:724–34.
[4] Wilson J, Burgh G. Energizing our future: rational choices for the 21st Century. Wiley Interscience; January 2008.
[5] Statistics–International energy Agency (IEA) key word statistics 2008. Available at: http://www.iea.org/textbase/nppdf/free/2008/key_stats_2008.pdf, [accessed 11.02.10].
[6] Pearce JM. Photovoltaics — a path to sustainable futures. Futures 2002;34 (7):663–74.
[7] Pearce JM. Expanding photovoltaic penetration with residential distributed generation from hybrid solar photovoltaic and combined heat and power systems. Energy 2009;34:1947–54.

[8] Trends in photovoltaic applications: survey report of selected IEA countries between 1992 and 2008. Report IEA-PVPS T1–18, Available at: http://www.iea-pvps.org/products/download/rep1_18.pdf; 2009 [accessed 11.02.10].
[9] Makrides G, Zinsser B, Norton M, Georghiou GE, Schubert M, Werner JH. Potential of photovoltaic systems in countries with high solar irradiation. Renewable and Sustainable Energy Reviews 2010;14:754–62.
[10] Raugei M, Frankl P. Life cycle impacts and costs of photovoltaic systems: current state of the art and future outlooks. Energy 2009;34:392–9.
[11] Feltrin V, Freundlich A. Material considerations for terawatt level deployment of photovoltaics. Renewable Energy 2008;33:180–5.
[12] Andersson BA, Azar C, Holmberg J, Karlsson S. Material constraints for thin-film solar cells. Energy 1998;23(5):407–11.
[13] Fthenakis V. Sustainability of photovoltaics: the case for thin-film solar cells. Renewable and Sustainable Energy Reviews 2009;13:2746–50.
[14] Intergovernmental Panel on Climate Change (IPCC), Climate change 2001: mitigation. Available at: http://www1.ipcc.ch/ipccreports/tar/wg3/index.htm, [accessed 11.02.10].
[15] Soro YM, Abramov A, Gueunier-Farret ME, Johnson EV, Longeaud C, Roca i Cabarrocas P, et al. Device grade hydrogenated polymorphous silicon deposited at high rates. Journal of Non-Crystalline Solids 2008;354:2092–5.
[16] Matsuda A, Takai M, Nishimoto T, Kondo M. Control of plasma chemistry for preparing highly stabilized amorphous silicon at high growth rate. Solar Energy Materials & Solar Cells 2003;78:3–26.
[17] Kakiuchi H, Matsumoto M, Ebata Y, Ohmi H, Yasutake K, Yoshii K, et al. Characterization of intrinsic amorphous silicon layers for solar cells prepared at extremely high rates by atmospheric pressure plasma chemical vapor deposition. Journal of Non-Crystalline Solids 2005;351:741–7.
[18] Mahan AH, Xu Y, Iwaniczko E, Williamson DL, Nelson BP, Wang Q. Amorphous silicon films and solar cells deposited by HWCVD at ultra-high deposition rates. Journal of Non-Crystalline Solids 2002;299-302:2–8.
[19] Sherwani AF, Usmani JA, Varun. Life cycle assessment of solar PV based electricity generation systems: a review. Renewable and Sustainable Energy Reviews 2010;14:540–4.
[20] Emery KA. Solar simulators and I-V measurement methods. Solar Cells 1986;18:251–60.
[21] Green M. Solar cells: operating principles, technology and system applications. Kensington: University of New South Wales; 1992.
[22] Staebler DL, Wronsky CR. Reversible conductivity changes in discharge-produced amorphous Si. Applied Physics Letters 1977;31:292.
[23] Roca i Cabarrocas P, Hamma S, Sharma SN, Viera G, Bertran E, Costa J. Nanoparticle formation in low-pressure silane plasmas: bridging the gap between a-Si:H and μc-Si films. Journal of Non-Crystalline Solids 1998;227-230:871–5.
[24] Kail F. Etude in-situ par ellipsométrie et spectrométrie de masse du transport de l'hydrogène dans a-Si:H: Cinétique de diffusion et modifications de structure. PhD thesis. Palaiseau: Ecole Polytechnique; October 21, 2005.
[25] Roca i Cabarrocas P. Plasma enhanced chemical vapor deposition of amorphous, polymorphous and microcrystalline silicon films. Journal of Non-Crystalline Solids 2000;266-269:31–7.
[26] Dadouche F, Béthoux O, Gueunier-Farret ME, Johnson E V, Roca i Cabarrocas P, Marchand C, Kleider JP. Geometrical optimization and electrical performance comparison of thin-film tandem structures based on pm-Si:H and μc-Si:H using computer simulation.
[27] Veneri PD, Aliberti P, Mercaldo LV, Usatii I, Privato C. Influence of microcrystalline silicon bottom cell on micromorph tandem solar cell performance. Thin Solid Films 2008;516:6979–83.
[28] Longeaud C, Kleider JP, Roca i Cabarrocas P, Hamma S, Meaudre R, Meaudre M. Properties of a new a-Si:H-like material: hydrogenated polymorphous silicon. Journal of Non-Crystalline Solids 1998;227–230:96–9.
[29] Butté R, Meaudre R, Meaudre M, Vignoli S, Longeaud C, Kleider JP, et al. Some electronic and metastability properties of a new nanostructured material: hydrogenated polymorphous silicon. Philosophical Magazine B 1999;79:1079–95.
[30] Meaudre M, Meaudre R, Butté R, Vignoli S, Longeaud C, Kleider JP, et al. Midgap density of states in hydrogenated polymorphous silicon. Journal of Applied Physics 1999;86:946–51.
[31] Kleider JP, Longeaud C, Gauthier M, Meaudre M, Meaudre R, Butté R, et al. Very low densities of localized states at the Fermi level in hydrogenated polymorphous silicon from capacitance and space-charge-limited current measurements. Applied Physics Letters 1999;75:3351–3.
[32] Stangl R, Froitzheim A, Kriegel M, Brammer T, Kirste S, Elstner L, et al. AFORS-HET, a numerical PC-program for simulation of heterojunction solar cells. In: Proceedings of the 19th European Photovoltaic Solar Energy Conference 2004; 1497–1500.
[33] Smith DM. Engineering computation with MATLAB. 2nd ed. Addison-Wesley; 2009.
[34] Cotts EJ. Hydrogenated amorphous silicon. In: Solid State Ionic1992, vol. 57. Cambridge: University Press; 1991 (Issues 1–2)173.
[35] Martins R, Fantonia A, Vieira M. Tailoring defects on amorphous silicon PIN devices. Journal of Non-Crystalline Solids 1993;164-166:671–4.
[36] Chatterjee P. Photovoltaic performance of a-Si:H homojunction p-i-n solar cells: a computer simulation study. Journal of Applied Physics 1994;76(2):1301.
[37] Liao CC. Genetic k-means algorithm based RBF network for photovoltaic MPP prediction. Energy 2010;35(2):529–36.
[38] Schultz AM, Sullivan CR. Voltage Converter with Coupled Inductive Windings and Associated Methods. US Patent Number 6.362.086. Volterra semiconductor Corp 2002.
[39] Li J, Sullivan CR, Schultz AM. Coupled Inductor design optimization for Fast Response low Voltage DC-DC Converter. In: Proceedings of the 17th IEEE Applied Power Electronics Conference and Exposition 2002; 2: 817–823.
[40] Zumel P, Garcia O, Cobos JA, Uceda J. Magnetic Integration for Interleaved Converters. In: Proceedings of the 18th IEEE Applied Power Electronics Conference and Exposition 2003; 2(9–13):1143–1149.
[41] Meynard T, Forest F, Labouré E, Costan V, Cunière A, Sarraute E. Monolithic Magnetic Couplers for Interleaved Converters With High Number of Cells. In: Proceedings of the 4th IEEE International Conference on Integrated Power Systems 2006.
[42] Forest F, Meynard T, Labouré E, Costan V, Cunière A, Martiré T. Optimization of supply voltage system in interleaved converters using intercell transformers. IEEE Transactions on Power Electronics 2007;22(3):934–42.